agronomy

MDPI

Article

Volatile-Based In-Field Screening of *Xylella fastidiosa* in Olive Plants Using a Smart E-Nose

Rossella Manganiello [1,*], Antonio Matere [2], Lavinia Moscovini [1], Corrado Costa [1], Federico Pallottino [1], Simone Vasta [1], Simone Figorilli [1], Nicoletta Pucci [2], Stefania Loreti [2], Simona Violino [1], Giuseppe Tatulli [2] and Francesca Antonucci [1]

[1] Centro di Ricerca Ingegneria e Trasformazioni Agroalimentari, Consiglio per la Ricerca in Agricoltura e L'analisi Dell'Economia Agraria (CREA), Via della Pascolare 16, Monterotondo, 00015 Rome, Italy; lavinia.moscovini@crea.gov.it (L.M.); corrado.costa@crea.gov.it (C.C.); federico.pallottino@crea.gov.it (F.P.); simone.vasta@crea.gov.it (S.V.); simone.figorilli@crea.gov.it (S.F.); simona.violino@crea.gov.it (S.V.); francesca.antonucci@crea.gov.it (F.A.)

[2] Centro di Ricerca Difesa e Certificazione, Consiglio per la Ricerca in Agricoltura e L'analisi Dell'Economia Agraria (CREA), Via Carlo Giuseppe Bertero 22, 00156 Rome, Italy; antonio.matere@crea.gov.it (A.M.); nicoletta.pucci@crea.gov.it (N.P.); stefania.loreti@crea.gov.it (S.L.); giuseppe.tatulli@crea.gov.it (G.T.)

* Correspondence: rossella.manganiello@crea.gov.it

Abstract

Xylella fastidiosa (*Xf*) is among the most devastating phytosanitary threats to Mediterranean agriculture, causing Olive Quick Decline Syndrome (OQDS). Since containment efficacy depends on timely intervention, scalable in-field screening tools are needed. This study evaluates a portable digital electronic nose, based on a carbon-nanotube sensor array combined with artificial intelligence algorithms, for the in-field screening of *Xf* through volatile organic compound (VOC) profiling. Three replicate acquisitions were performed on 130 olive trees (390 measurements) across four cultivars (Cellina di Nardò, Ogliarola Salentina, Ogliarola Barese, and Leccino) in four Italian regions (Apulia, Calabria, Lazio, and Tuscany). Plant status was assigned from the official status of the sampling area (demarcated OQDS focus versus *Xf*-free area) and supported by real-time quantitative PCR (qPCR) on every plant; within demarcated sites, plants with undetectable DNA in sampled twigs were retained as *Xf*+ following phytosanitary criteria, giving 216 infected and 174 healthy samples. The multidimensional sensor signals were processed with an optimized Shallow Neural Network. Under plant-grouped 80/20 validation, keeping each plant's replicates in the same subset, the model achieved (93.3 ± 4.0)% accuracy, (97.7 ± 3.5)% sensitivity, and (88.2 ± 8.3)% specificity (mean ± SD). A feature-importance analysis revealed a reproducible, though not chemically resolved, VOC-related response pattern. This low-cost, portable Internet of Things (IoT) device offers a proof-of-concept screening approach for *Xf* surveillance, pending plant-level and external validation.

Keywords: volatile organic compounds (VOCs); digital electronic nose; digital smart agriculture; phytosanitary surveillance; Artificial Neural Networks (ANNs)

Academic Editor: Jayme Garcia Arnal Barbedo

Received: 28 July 2026
Revised: 25 August 2026
Accepted: 28 August 2026
Published: 29 August 2026

1. Introduction

Xylella fastidiosa comprises several subspecies of phytopathological relevance, among which *fastidiosa*, *pauca*, and *multiplex* are the most frequently reported worldwide. *Xylella fastidiosa* subsp. *pauca* (*Xfp*) has emerged as one of the most devastating plant pathogens affecting Mediterranean agriculture, with Italy representing the epicenter of its impact

on olive cultivation. Since its first detection in Apulia in 2013, the bacterium has caused the widespread Olive Quick Decline Syndrome (OQDS), characterized by rapid leaf, twig, and branch die-back leading to tree collapse [1]. The *Xf* subspecies *multiplex* and *fastidiosa* have subsequently been detected in Italy, with *multiplex* occurring in Tuscany, Lazio, and Apulia [2], whereas *fastidiosa* has so far been reported only in Apulia [3]. These subspecies differ in host range, geographic distribution, and sequence types, contributing to the complexity of surveillance and containment strategies in affected regions [4]. The pathogen is primarily transmitted by xylem-feeding insects such as *Philaenus spumarius*, enabling fast dissemination across olive-growing regions [5]. In Apulia, the local olive cultivars Ogliarola Salentina and Cellina di Nardò are highly susceptible to *Xfp*, leading to the severe decline of centuries-old olive groves and posing a serious threat to both regional biodiversity and the local economy, which relies heavily on olive oil production [6]. These cultivars are among the richest in polyphenol content and are known to produce oils with exceptionally high nutritional value, making their loss particularly impactful [7].

Efforts to manage the epidemic include monitoring resistant cultivars, such as 'Leccino', which show promising tolerance traits under a high inoculum pressure [8]. Remote sensing and satellite-based surveying have also been explored to assess grove health and support early intervention strategies [9].

Within the framework of digital agriculture, the integration of smart Internet of Things (IoT) devices is increasingly applied to plant disease containment. The wider adoption of these approaches for the early detection of *Xf* in olive orchards is often constrained by weather dependency, environmental operating conditions, regulatory hurdles, and labor-intensive sampling. IoT-connected physiological and environmental sensors have been deployed on *Xf*-infected olive trees to monitor the tree response to infection and therapy [10], although not as volatile-sensing systems. In the study of Castrignanò et al. [11], the application of an integrated approach of various statistical and spatial geostatistical techniques was used to early discriminate asymptomatic and/or infected plants, by using radiometric data collected with a multispectral sensor onboard a drone. Di Nisio et al. [12] showed that multispectral imagery from a mid-sized rotary-wing UAV can successfully assess olive tree health in near-real-time in relation to OQDS caused by *Xfp*. In addition, the primary objective of the study of Román-Écija et al. [13] was to characterize the host-pathogen interactions between distinct *Xf* strains and local Spanish olive cultivars using a handheld leaf spectrometer. This approach validated proximal sensing as a promising, non-invasive tool for early disease detection and risk mitigation management.

The focus of this study is to highlight how advanced sensor-based technology, such as the digital electronic nose (e-nose), can offer useful tools for the in-field smart screening of *Xf* infected olive trees. These portable, low-cost IoT systems can help identify infected plants by detecting the volatile organic compounds (VOCs) changes associated with disease development [14–16]. This electronic nose operates as a high-dimensional data source, yielding extensive and dense datasets that capture the intricate volatile profiles of infected plants. The integration of Artificial Intelligence (AI) algorithms allows for the seamless handling of high-dimensional datasets, optimizing the screening and detection of *Xfp* infections in olive orchards. In this context, the Artificial Neural Networks (ANNs), the Shallow Neural Networks (SNNs), represent a good solution for processing the complex and multidimensional patterns generated by the e-nose [17,18]. Due to their computationally streamlined architecture, SNNs can effectively decode non-linear variations in VOCs while preventing overfitting and minimizing hardware resource requirements. This high algorithmic efficiency enables their direct integration into edge-computing smart devices and portable IoT systems for real-time monitoring. Consequently, SNNs represent a promising approach for rapid, in-field classification of olive phytosanitary status.

In this study, the Smell Inspector (SmartNanotubes Technologies GmbH, Dresden, Germany), a portable carbon-nanotube electronic nose [19], was used in combination with AI algorithms to compare the VOC emission of healthy and diseased olive plants directly in the field. Generally, this system works by capturing subtle changes in smell patterns and turning them into digital signals that can be analyzed [20,21]. As a result of its lightweight design and low energy use, it can be easily integrated into portable devices or continuous monitoring systems. Specifically, a digital e-nose was deployed directly in the field to detect variations in VOC profiles, comparing healthy plants with diseased ones, whose phytosanitary state was confirmed by molecular analysis. This approach aims to provide an efficient, low-cost, and portable screening system for detecting *Xf*-infected olive trees directly in the field, thereby supporting rapid containment and sustainable management strategies against this devastating pathogen.

2. Materials and Methods

2.1. Data Collection

A total of 390 measurements were collected, using the Smell Inspector e-nose in different Italian regions (i.e., Apulia, Calabria, Lazio, and Tuscany; Figure 1). In particular, plants analyzed in the OQDS-free areas of Calabria, Lazio, and Tuscany did not show any symptoms, whereas plants analyzed in Apulia were located within the OQDS-affected olive orchards (Figure 1). The primary class label was assigned on an orchard basis (*Xf*+ = plant located inside a demarcated OQDS focus; *Xf*− = plant located in an *Xf*-free area). Real-time quantitative PCR (qPCR) [22] on pooled twigs was performed on every plant as molecular confirmation of the assigned label (*Xf*+/*Xf*−) used as the reference classification throughout the manuscript. Bacterial DNA was quantified by qPCR on pooled twigs of each plant. All 58 plants from the unaffected sites returned undetectable bacterial DNA. Among the 72 plants sampled in the OQDS-affected orchards, 8 showed no detectable *Xfp* DNA in the twigs analyzed. Nevertheless, these plants were still assigned to the *Xf*+ group, since, in infected areas, a plant may be considered infected even when the pathogen is not detected in a single sample. Indeed, *Xfp* exhibits a discontinuous and uneven distribution within the canopy, particularly during the early stages of infection, and may therefore escape detection in an individual sampled twig. On this basis, the samples were classified into two main experimental groups (216 *Xf*+ and 174 *Xf*−; Table 1). Field symptom-severity scores, independently recorded by the plant-pathology team, were not used in this classification, so the *Xf*+ group cannot be assumed to be asymptomatic.

Table 1. Overview of the olive tree sampling dataset analyzed by the Smell Inspector e-nose for VOCs discrimination. The phytosanitary status (*Xylella fastidiosa*-diseased *Xf*+ vs. healthy *Xf*−), geographic distribution, and specific cultivars (CV) analyzed in this study are reported; the OQDS status of the sampling site is indicated by the Geographic Origin column; N plants × 3 replicates = Smell acquisitions.

Plant Status	Label	Geographic Origin	Region (Province)	CV	N Plants	Replicates	Smell Acquisitions	Coordinates
Xf+	A1CE	Field 1 Alezio	Apulia (Lecce)	Cellina di Nardò	14	3	42	40°01′58.1″ N 18°03′59.0″ E
	A1OS	Field 1 Alezio	Apulia (Lecce)	Ogliarola Salentina	15	3	45	40°01′58.1″ N 18°03′59.0″ E
	P2CE	Field 2 Parabita	Apulia (Lecce)	Cellina di Nardò	1	3	3	40°03′33.3″ N 18°07′41.3″ E
	P2OS	Field 2 Parabita	Apulia (Lecce)	Ogliarola Salentina	4	3	12	40°03′33.3″ N 18°07′41.3″ E
	U3CE	Field 3 Uggiano La Chiesa	Apulia (Lecce)	Cellina di Nardò	26	3	78	40°06′31.8″ N 18°26′42.3″ E

Table 1. *Cont.*

Plant Status	Label	Geographic Origin	Region (Province)	CV	N Plants	Replicates	Smell Acquisitions	Coordinates
Xf+	U4CE	Field 4 Uggiano La Chiesa	Apulia (Lecce)	Cellina di Nardò	2	3	6	40°07′22.9″ N 18°27′55.0″ E
	U4OS	Field 4 Uggiano La Chiesa	Apulia (Lecce)	Ogliarola Salentina	3	3	9	40°07′22.9″ N 18°27′55.0″ E
	OSOS	Pantanelli Ostuni	Apulia (Brindisi)	Ogliarola Salentina	7	3	21	40°43′17.1″ N 17°34′56.7″ E
Sub-total (*Xf*+)				**72**			**216**	
Xf−	LRCE	CRSFA Locorotondo	Apulia (Bari)	Cellina di Nardò	10	3	30	40°45′16.07″ N 17°20′22.89″ E
	LROB	CRSFA Locorotondo	Apulia (Bari)	Ogliarola Barese	10	3	30	40°45′16.07″ N 17°20′22.89″ E
	MTCE	CREA-OFA Mirto	Calabria (Cosenza)	Cellina di Nardò	10	3	30	39°37′06.4″ N 16°46′22.5″ E
	MTOS	CREA-OFA Mirto	Calabria (Cosenza)	Ogliarola Salentina	8	3	24	39°37′06.4″ N 16°46′22.5″ E
	RMLE	CREA-DC Roma	Lazio (Roma)	Leccino	10	3	30	41°55′57.50″ N 12°33′14.78″ E
	FILE	SEMIA Calenzano	Tuscany (Florence)	Leccino	10	3	30	43°52′3.41″ N 11°9′12.72″ E
Sub-total (*Xf*−)				**58**			**174**	
TOTAL				**130**			**390**	

Figure 1. Geographic distribution of olive sampling sites. The map illustrates the locations of healthy plants (magenta symbols) and *Xylella fastidiosa*-diseased plants (orange dots), as confirmed by qPCR. Diseased samples originate from infected focus areas within the Apulia region (Provinces of Lecce and Brindisi), including Alezio, Parabita, Uggiano La Chiesa, and Ostuni. Healthy samples were collected from distinct reference centers and regions: CRSFA Locorotondo (Apulia, BA), CREA-OFA Mirto (Calabria, CS), CREA-DC Rome (Lazio, RM), and SEMIA Calenzano (Tuscany, FI).

The cultivars analyzed were Ogliarola Salentina, Ogliarola Barese, Cellina di Nardò, and Leccino. The plants were assessed both under open-field conditions and in pots (the latter only for samples from LRCE and LROB, Table 1), and at different ages and phenological stages. The age of trees, the agronomic management, and the environmental conditions at the time of sampling were neither controlled nor recorded. Healthy trees of the susceptible cultivars are no longer available inside the Salento infected area, so that *Xf*− references necessarily had to be sampled in *Xf*-free regions. The phytosanitary status (*Xf*+ or *Xf*−) is partially confounded with the sampling site and acquisition time, since healthy and infected samples necessarily originated from different geographical areas. Consequently, temperature and humidity varied across measurements. The comparison between *Xf*+ and *Xf*− plants was instead based on cultivar: Cellina di Nardò and Ogliarola salentina were sampled in both phytosanitary conditions, whereas Ogliarola Barese and Leccino were sampled only among the *Xf*− plants. The study was thus designed to test whether a VOC-based discrimination is detectable across the broad variability of age, management, and different field conditions that characterize real olive orchards.

Although the e-nose screening is intended as a non-destructive in-field method, in the present validation, the twigs were excised to allow each measurement to be paired with qPCR confirmation on the same material. For each sample, three twigs of about two years old, together with their leaves, were cut, coarsely chopped, and immediately placed inside a bell-shaped glass container, whose headspace was then analyzed with the e-nose (Figure 2). Each acquisition comprised three consecutive 5 min replicates.

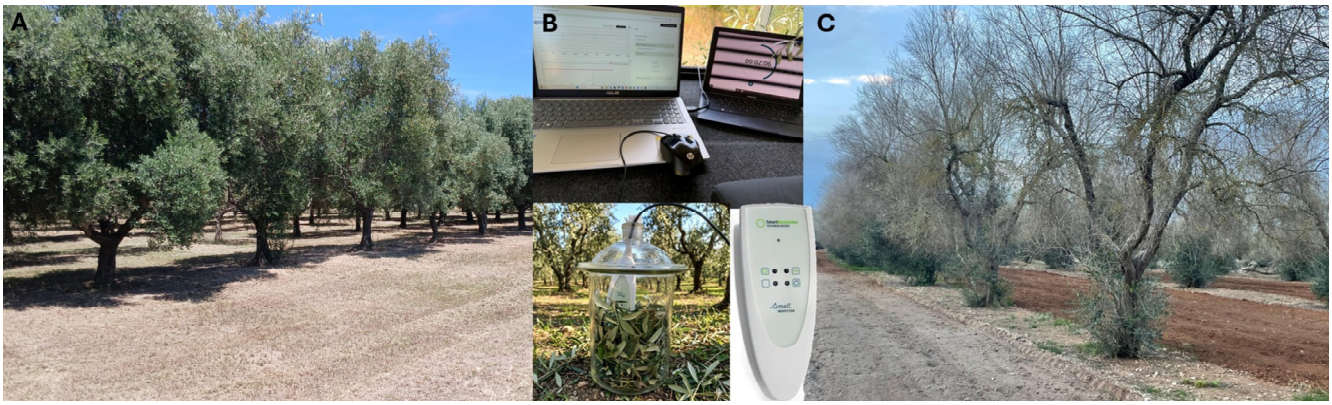

Figure 2. Experimental field design for VOC acquisition through Smell Inspector e-nose: (**A**) healthy plot before *Xylella fastidiosa* infection (Mirto (CS), Calabria); (**B**) in-field experimental setup for VOC acquisition from branch samples using the portable e-nose within sampling glass container and data acquisition station (laptop and tablet running analysis software); and (**C**) diseased plot containing olive trees infected by *Xf*, exhibiting canopy decline, yellowing, and sparse foliage (Uggiano La Chiesa (LE), Apulia).

2.2. E-Nose

The Smell Inspector (SmartNanotubes Technologies GmbH, Dresden, Germany) is a portable nonspecific digital electronic nose designed for real-time VOC digitization. The device integrates four Smell iX16 multichannel gas-sensor chips, each housing sixteen chemiresistive sensing channels based on semiconducting carbon-nanotube (CNT) nanomaterials, for a total of 64 channels. The electrical resistance of each channel is recorded every 1.8 s, together with ambient temperature and relative humidity. The chemiresistive sensing mechanism relies on shifts in the electrical resistance of the functionalized CNT thin films upon adsorption of volatile organic compounds at the molecular level. Unlike conventional metal-oxide sensors, the CNT-based technology functions efficiently at room temperature, with a maximum device power consumption of 0.28 W (enabling battery-powered field operation) and detection sensitivity in the parts-per-billion (ppb)

range [19,23]. Each chip provides sixteen channels, comprising both chemically functionalized sensing elements, each exhibiting a cross-reactive response profile to diverse gas compositions, and unfunctionalized reference elements; the resulting multivariate signal constitutes a multidimensional digital smell fingerprint that can be processed by machine-learning algorithms for odor pattern recognition and classification. The high surface-to-volume ratio inherent to CNT nanomaterials promotes rapid sensor response upon VOC exposure, supporting near-real-time monitoring; however, recovery times may extend from one to several minutes depending on the nature and concentration of the analyte [24]. The compact form factor of the device (166 × 64 × 31 mm; 130 g) and dual power supply options (USB Micro-B or AAA batteries) support portable field deployment. The Smell Inspector has an estimated cost of €489 (including 19% VAT) and requires no per-sample reagents or dedicated laboratory infrastructure, in contrast to the equipment and consumables needed for laboratory qPCR. Data transmission via USB or Bluetooth enables integration into custom acquisition pipelines, and the open software architecture allows user-defined training for application-specific VOCs classification.

Of the 64 available channels, 19 are non-functionalized reference (baseline) channels, labeled "999", which exhibit no response to volatile compounds and were therefore excluded from all analyses. The remaining 45 active channels are organized into groups of three sensors sharing the same chemical functionalization, providing built-in replicate redundancy to reduce intra-sensor variability. Responses within each triplicate group were averaged to yield 15 canonical features, each expressed as the fractional resistance change $\Delta R/R_0$, where R_0 is the baseline resistance and R is the resistance varying during exposure to the sample headspace. The same signal-extraction routine was applied identically to every sample and to its matched blank, so that all acquisitions are directly comparable.

Prior to data acquisition, the device was powered on and allowed to stabilize for approximately 30 min, as recommended by the manufacturer, to ensure thermal and electrical equilibrium of the CNT sensor array and minimize baseline drift. The Smell Inspector was then connected to the Smell Annotator software (SmartNanotubes Technologies, GmbH, Dresden, Germany; version 1.5.0) via USB.

Each plant was analyzed in three consecutive 5 min replicate acquisitions following the same acquisition protocol (about 20 min per plant, including sensor recovery between replicates); the triplicate acquisitions were used for model training and validation, whereas operational in-field screening would rely on a single 5 min acquisition per plant. For each replicate, a matched blank measurement was acquired using the empty sealed jar under identical conditions. The 15 features of each replicate were blank-corrected by subtracting the corresponding blank features, eliminating contributions from the glass container and the surrounding environment. Environmental temperature and relative humidity were continuously logged throughout each acquisition and monitored during post-processing to account for potential humidity-mediated effects on CNT conductivity.

Raw data were exported from the *Smell Annotator* in CSV format. After exclusion of inactive channels (labeled 999), $\Delta R/R_0$ was computed for each of the 45 active channels and the 15 canonical features were derived by averaging triplicates within each functionalization group. These 15 features constitute the multidimensional digital smell fingerprint of each sample and were used as input variables for chemometric analysis. The 45 individual active channels, prior to triplicate averaging, were instead used as input variables for the Shallow Neural Network, so as to preserve the residual information carried by the within-triplicate variability.

2.3. Xylella Fastidiosa Analyses

The entire procedure from sample collection, to DNA extraction and qPCR were performed following the European Plant Protection Organization recommendations EPPO

standard PM7/24 (5), specifically the real-time qPCR test of Harper et al. described in its Appendix 5 [25]. In particular, each sample was collected from the medial portion of each plant for a total of four samplings per plant at four cardinal points constituting a pooled twigs sample with mature leaves. Leaf tissues (petiole, midrib, and basal portion) were processed using the QuickPick™ SML Plant DNA Kit (Bio-Nobile, Turku, Finland), coupled with the KingFisher automated extraction platform (Thermo Fisher Scientific, Waltham, MA, USA) (Leaf-QuickPick). Each sample was assessed in duplicate by the qPCR according to Section 3.5.5 of the IPPC diagnostic protocol DP 25 for *Xylella fastidiosa* [22].

2.4. Statistical Analysis

A preliminary Principal Component Analysis (PCA) was performed on the VOC profiles of olive samples, categorized by geographic origin and phytosanitary status (i.e., *Xf* diseased vs. healthy; Table 1), to explore the general clustering and underlying structure of the dataset. The high-dimensional response from the 45-channel digital e-nose was reduced into a lower-dimensional space to assess group separation [26]. The results are visualized via biplots, integrating both factor scores, representing the projection of sample centroids within the principal component (PC) space, and loadings, which depict the relative contribution and correlation of each sensing channel to the explained variance. The magnitude of the eigenvalues, expressed as a percentage of the total explained variance for each principal axis, was reported to evaluate the model's representativeness.

2.5. Artificial Intelligence Algorithms

An Artificial Neural Network (ANN) approach based on a Shallow Neural Network (SNN) was used to discriminate diseased and healthy samples according to the VOCs identified with the e-nose. In general, a feed-forward neural network comprises three main layers: an input layer composed of nodes corresponding to the features selected, i.e., the 45 active channels; one or more hidden layers (fully connected hidden layers optimized with a varying number of neurons, determined via grid search); and the output layer composed of nodes corresponding to the number of classes to recognize (Figure 3).

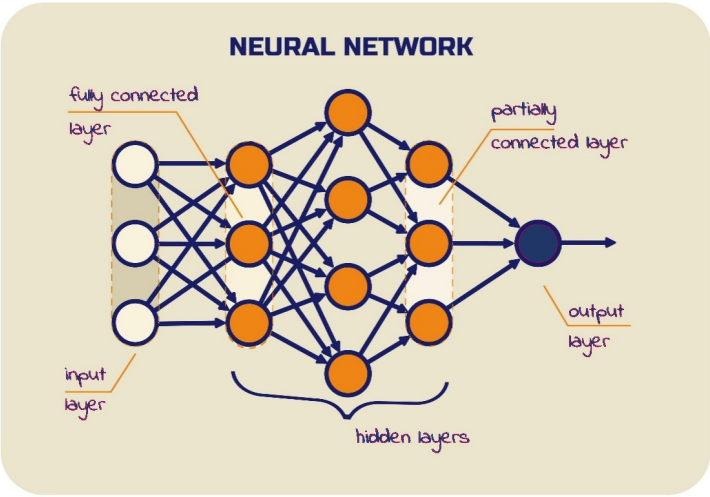

Figure 3. General, illustrative neural network computational model scheme that consists of interconnected nodes, called neurons, which are organized in layers. The nodes are connected to the nodes in the next layer, creating a network. The first layer is the input layer, followed by hidden layers, and the last layer is the output layer.

In particular, the SNN implemented in this study was characterized by the following: an input layer composed of nodes corresponding to the selected discriminant VOC features

extracted from the e-nose sensors; a single hidden layer with 200 neurons, iteratively determined during the training by minimizing the sparse categorical cross entropy, used as loss function, between true and predicted data, and utilizing the Rectified Linear Unit (ReLU) activation function to capture non-linear relationships within the odor profiles; and a binary classification output layer employing a Softmax (normalized exponential function) activation function to compute the probability of a sample belonging to either the "healthy" or "diseased" class [27].

The network was trained using a supervised learning approach with the root mean square propagation algorithm (RMSProp), with a 0.001 learning rate, as optimizer. To prevent overfitting and ensure model generalizability across the different geographic origins and olive cultivars (Cellina di Nardò, Ogliarola Salentina, Ogliarola Barese, and Leccino), an early stopping callback—that interrupts the process when the accuracy is maximized—was applied during training to determine the number of epochs in each repetition (on average, approximately 100 epochs, range 62–132). The network was evaluated under a plant-grouped 80/20 split, in which all three replicate acquisitions of a plant were kept in the same subset to prevent information leakage between replicates; the split was repeated twenty times and performance is reported as mean ± standard deviation. Prior to training, the input features were standardized to zero mean and unit variance using statistics estimated on the training partition only and applied unchanged to the test partition, so that no test information influenced the scaling. For comparison, support vector machine (SVM), random forest (RF), and partial least squares discriminant analysis (PLS-DA) classifiers were evaluated under the same scheme. A sensitivity analysis was also performed in which the eight qPCR-negative *Xf*+ plants were, alternatively, excluded or reassigned to the healthy class. The classification performance of the SNN model was evaluated using standard binary-classification metrics, including overall accuracy, precision, sensitivity (recall), and F1-score [28,29]. All metrics were derived from the confusion matrices of the training and test subsets, where true positives (TPs) and false negatives (FNs) refer to *Xf*+ samples and true negatives (TNs) and false positives (FPs) to *Xf*− samples. Diagnostic sensitivity was computed as TP/(TP + FN), i.e., the proportion of *Xf*+ plants correctly classified, and diagnostic specificity as TN/(TN + FP), i.e., the proportion of *Xf*− plants correctly classified. Diagnostic specificity therefore coincides with the recall of the *Xf*− class, and diagnostic sensitivity with the recall of the *Xf*+ class. Per-class precision was computed as TP/(TP + FP), the F1-score as the harmonic mean of precision and recall, and overall accuracy as (TP + TN)/(TP + TN + FP + FN); the reported F1-score is the macro-average of the two per-class values.

The SNN model was developed in Python v3.9.18 using Keras API [30] for TensorFlow [31] library and scikit-learn [32] metrics to assess the performance.

3. Results

Figure 4 reports the PCA biplot of the VOC profiles extracted from olive samples, analyzed via the Smell Inspector e-nose. The first two principal components (PC1 and PC2) explain a cumulative variance of 85.5% (with PC1 accounting for 74.4% and PC2 for 11.1%), indicating that the biplot captures most of the variance of the dataset. The score plot reveals a visible separation along the PC1 axis between two main clusters:

- Healthy plants (magenta dots): grouped predominantly on the positive side of PC1 (quadrants I and IV), particularly represented by samples like MTOS, MTCE, LROB, LRCE, and FILE;
- Infected plants (orange dots, *Xylella fastidiosa*): mostly distributed along the negative side of PC1 (quadrants II and III), such as P2CE, P2OS, U4OS, and U3CE. One healthy

(*Xf*−) sample, RMLE, projected atypically onto this negative side, overlapping with the infected cluster.

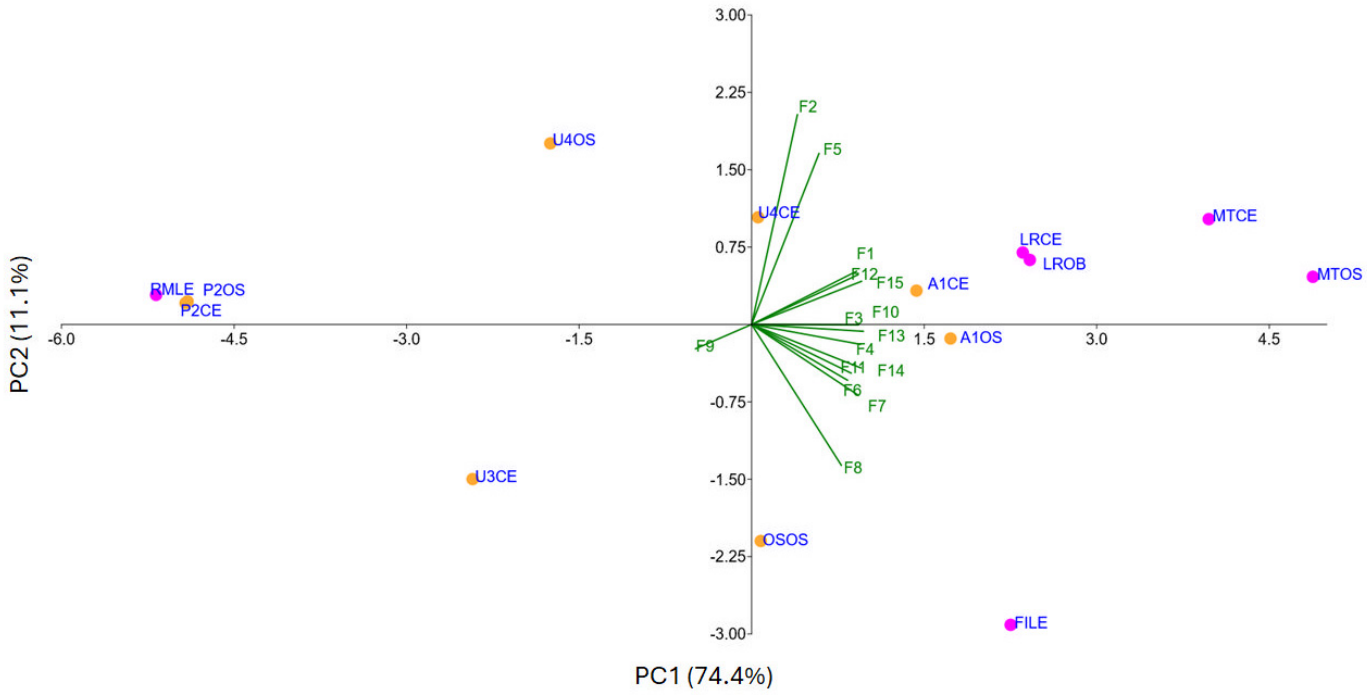

Figure 4. PCA biplot of VOC profiles from olive samples analyzed with the Smell Inspector e-nose. Orange dots: *Xylella fastidiosa*-infected (diseased) plants. Magenta dots: healthy plants. Green vectors: loadings of the 15 VOC features (F1–F15) derived from the Smell Inspector sensor array. PC1 and PC2 account for 74.4% and 11.1% of the total variance, respectively.

The loading vectors (green lines, F1–F15) indicate that the majority of the VOC features (specifically F1, F3, F4, F7, F10, F11, F12, F13, F14, and F15) project toward the positive side of PC1. This strong positive alignment suggests that healthy olive samples tend to show higher values of these features along PC1, compared to the infected ones. Conversely, features F2 and F5 contribute heavily to the positive loading of PC2 (associated to U4CE and A1CE), whereas F8 strongly influences the negative direction of PC2 (associated to OSOS and FILE).

The ANN approach based on an SNN was evaluated under a plant-grouped design in which the three replicate acquisitions of each plant were kept in the same subset to avoid information leakage between replicates. Under plant-grouped 80/20 validation, the SNN achieved (93.3 ± 4.0)% accuracy, (97.7 ± 3.5)% diagnostic sensitivity, (88.2 ± 8.3)% specificity, (94.2 ± 3.3)% precision, and (93.2 ± 4.2)% F1-score (mean ± SD). Under the same scheme, the SNN performed comparably to the conventional classifiers (RF 93.6 ± 4.6%, SVM 83.2 ± 5.6%, and PLS-DA 80.2 ± 6.5% accuracy), while retaining the highest diagnostic sensitivity, a relevant metric for a pre-screening tool. Excluding the eight qPCR-negative *Xf*+ plants, or reassigning them to the healthy class, left the performance essentially unchanged (92.9 ± 3.7% and 89.7 ± 4.0% accuracy, respectively), confirming that these plants do not drive the classification. The other metrics indicate how often positive predictions are right (precision) and whether the model correctly identifies positive instances (recall). On the held-out test subset (n = 78 acquisitions, comprising 36 *Xf*− and 42 *Xf*+ samples in the representative partition of Figure 5), the model correctly classified 33 of the 36 *Xf*− and 40 of the 42 *Xf*+ acquisitions. Table 2 reports the detailed test-set metrics of the SNN under plant-grouped validation, and Table 3 compares them, under the same scheme, with those obtained by the conventional classifiers. The SNN achieved an accuracy comparable

to the best conventional model (RF, 93.6 ± 4.6%) but the highest diagnostic sensitivity (97.7 ± 3.5%), i.e., the greatest ability to correctly identify infected plants, which is the property of primary interest for a screening tool, whereas SVM and PLS-DA were markedly less accurate. Because the two classes are of comparable size, the reported F1-score is the macro-average of the two per-class values. The corresponding confusion matrices for a representative partition are shown in Figure 5.

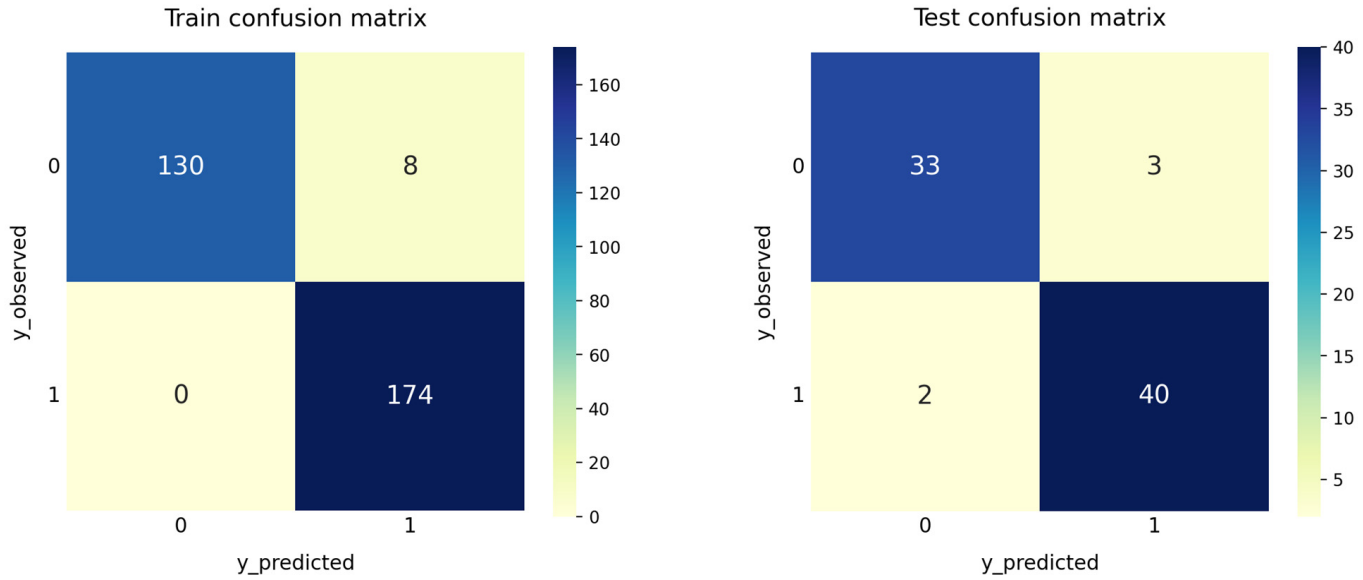

Figure 5. C. fusion matrices of the SNN under plant-grouped 80/20 validation, for a representative training (**Left**) and test (**Right**) partition (grouped by plant). Rows and columns represent the actual and predicted classes (0 = Healthy, *Xf*−; 1 = Diseased, *Xf*+).

Table 2. Detailed metrics for the Shallow Neural Network (SNN) under plant-grouped 80/20 validation (mean ± SD).

Metric	SNN Plant-Grouped 80/20 (Mean ± SD)
Test Accuracy	93.3 ± 4.0%
Diseased Recall (Sensitivity)	97.7 ± 3.5%
Diseased Precision	94.2 ± 3.3%
Healthy Recall (Specificity)	88.2 ± 8.3%
F1-score (macro)	93.2 ± 4.2%

Table 3. Comparison of the SNN with conventional classifiers under plant-grouped 80/20 validation (mean ± SD over 20 repetitions); all values are percentages.

Model	Accuracy	Sensitivity	Specificity	F1
SNN	93.3 ± 4.0	97.7 ± 3.5	88.2 ± 8.3	93.2 ± 4.2
RF	93.6 ± 4.6	94.4 ± 5.9	92.6 ± 6.5	94.0 ± 4.3
SVM	83.2 ± 5.6	88.8 ± 8.6	76.7 ± 8.4	85.0 ± 5.3
PLS-DA	80.2 ± 6.5	83.7 ± 8.0	76.1 ± 11.2	82.0 ± 5.8

Under plant-grouped 80/20 validation, the model retained a high diagnostic sensitivity (97.7 ± 3.5%), together with a specificity of 88.2 ± 8.3%. In the representative partition shown in Figure 5, the test set contained three false positives and two false negatives (91.7% specificity and 95.2% sensitivity in that partition), so both error types occurred; averaged over the twenty partitions, false negatives (diseased plants classified as healthy) were slightly less frequent than false positives (healthy plants classified as diseased). Since no plant contributes to both the training and test folds, this plant-grouped evaluation provides a realistic estimate of generalization.

VOC Fingerprinting and Feature Importance

The permutation importance of the SNN input channels, computed as the mean decrease in test accuracy when each channel was randomly permuted and averaged over the 20 plant-grouped repetitions, was used to explore the contribution of the individual sensing channels to the discrimination of *Xylella fastidiosa* infection (Figure 6). The 45 active channels correspond to the response of the sensor array to the blend of VOCs emitted by the olive plants. Because they are organized in triplicate groups sharing the same chemical functionalization, the importance profile is interpreted at the level of functionalization groups. No single channel dominated the ranking: the most consistently informative channel (Channel 9, among the five highest in 13 of the 20 repetitions) belonged to the ch9–ch11 triplet, while the remaining channels contributed comparable and variable amounts, so that the importance ranking alone cannot be read as a ranking of influence. The discriminant capacity of each triplet was therefore assessed separately, on the plant-level means of the three replicate acquisitions (130 plants), by means of the area under the Receiver Operating Characteristic (ROC) curve (AUC) and of the Mann–Whitney test. For all fifteen triplicates, the fractional resistance change was more negative in $Xf+$ than in $Xf-$ plants, with no reversal. Infection therefore amplifies the resistance drop over the whole functionalized portion of the array, although the magnitude of the effect differs markedly among triplicates. Over the complete dataset, the predominant contribution to the discrimination came from channels ch3–ch5 and ch9–ch11, with AUC = 0.731 and 0.730, respectively ($p < 0.001$), followed by ch60–ch62 (AUC = 0.667) and ch54–ch56 (AUC = 0.661). The neural network effectively filters the complex background noise of "healthy" plant emissions and to separate infected from healthy plants under varying environmental conditions. Overall, these results indicate that healthy and *Xf*-infected olive plants are associated with a reproducibly distinguishable volatile fingerprint, captured by the sensor array with a stable classification performance across the repeated plant-grouped partitions. Rather than depending on a single sensor, the discrimination arises from the distributed response of the array; two independent analyses, permutation importance and univariate AUC/Mann–Whitney testing, consistently identified the ch9–ch11 and ch3–ch5 channel groups as the most informative, indicating that specific functional regions of the array contribute preferentially to the separation.

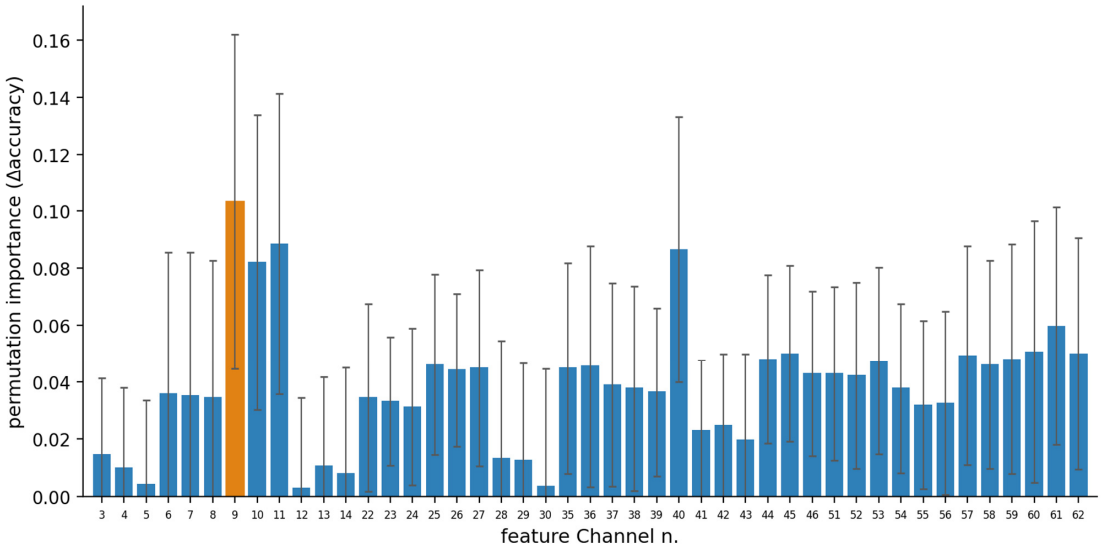

Figure 6. Permutation importance of the input channels for the SNN, computed as the mean decrease in test accuracy when each channel is randomly permuted, averaged over the 20 plant-grouped repetitions bars: mean; error bars: standard deviation). Channel 9 (highlighted in orange) was the most consistently informative channel; the importance is distributed across the 45 active sensing channels of the Smell Inspector array.

Because the device is cross-reactive and non-specific, these weights cannot be attributed to individual chemical compounds. Since all *Xf*+ plants were sampled in Apulia, the analysis was repeated on the Apulian subset alone, using the healthy trees of Locorotondo as controls (72 *Xf*+ and 20 *Xf*− plants). The discrimination did not decrease: the AUC increased for fourteen of the fifteen sensor triplicates, the largest separation being provided by channels ch6–ch8, whose AUC rose from 0.636 to 0.851, followed by ch3–ch5 (from 0.731 to 0.809) and ch9–ch11 (from 0.730 to 0.792). Had the classification been driven by the geographical origin of the samples, removing the between-region contrast would have reduced, and not improved, the separation.

4. Discussion

Currently, the diagnosis of *Xylella fastidiosa* is mainly based on the use of destructive tools, primarily relying on molecular assays. Complementary non-destructive approaches for OQDS monitoring, such as remote and satellite sensing, have recently been developed as early-warning systems; however, they mainly detect canopy changes occurring close to the onset of visible symptoms. Volatile compound profiling offers a complementary approach, since the metabolic alteration induced by *Xf* modifies the volatile fraction of olive tree tissues: Mentana et al. [33] identified more than one hundred volatile compounds in olive twigs using HS-SPME-GC-MS and reported a marked enrichment of methyl esters in *Xf*-infected material. This change in the volatile profile is consistent with other chemical alterations previously reported in infected olive trees, such as the accumulation of quinic acid and mannitol [34], the presence of specific metabolic markers associated with the disease and the cultivar [35], and the metabolic alterations that allowed asymptomatic Cellina di Nardò trees to be identified [36].

The electronic nose offers a significant advantage over these approaches, as it is based on simple and portable instrumentation that can be operated directly at the point of care, and its use for the early diagnosis of plant pathogens is already documented in the literature [15]. The diagnostic performance obtained in this study is consistent with that reported for diagnostic techniques based on volatile compounds in comparable pathogen systems. In citrus, Hazarika et al. [37] discriminated citrus tristeza virus (CTV)-infected mandarin plants using a custom-developed electronic nose; Xu et al. [38] similarly distinguished huanglongbing-infected trees using a low-cost gas sensor array, demonstrating that a non-specific "electronic nose" captures most of the diagnostic information contained in the complete profile of volatile compounds; Wang et al. [39] achieved an average accuracy of 95.83% for the early diagnosis of huanglongbing through untargeted metabolomics and machine learning, at a higher cost than that of a chemiresistive array. The same "Smell Inspector" device was able to distinguish wheat grains infected with *Fusarium graminearum* and *F. culmorum* [21] and to detect tomato spotted wilt virus infection in a preliminary trial [20], indicating that the array responds to bacterial, fungal, and viral infections through a unified and distributed mechanism. The same literature, however, consistently reports that e-nose responses are strongly modulated by the sampling procedure, the phenological stage of the plant, the temperature and relative humidity, and the sensor drift, and that gas-sensor arrays generally show a lower analytical sensitivity and specificity than microbiological and molecular methods [15,40,41].

To the best of the authors' knowledge, this is the first study to apply a room-temperature carbon-nanotube electronic nose combined with a neural network classifier to the volatile-based detection of *Xylella fastidiosa* directly in commercial olive orchards. The in-field detection of the pathogen has previously been approached through proximal and remote sensing and through portable molecular or biosensing devices. A chemiresistive volatile-sensing array has not previously been applied in this context, although, in the

present validation, VOC sampling required twig excision rather than a fully non-destructive protocol. A *Xf*-associated volatile signature in olive twigs had, however, already been demonstrated by gas chromatography–mass spectrometry [33].

This study shows the potential of the Smell Inspector e-nose combined with an AI-based algorithm, specifically an SNN, for the in-field discrimination of healthy and *Xf*-diseased olive trees. The exploratory PCA already indicated a trend towards class separation along the first principal component, with healthy samples projecting predominantly on its positive side and infected ones on the negative side; however, the partial overlap between the two groups, including the occasional healthy sample (e.g., RMLE) projecting among the infected ones, shows that an unsupervised linear projection does not fully resolve the phytosanitary status, and justifies the use of the supervised SNN to capture the non-linear structure of the volatile response. The training and test accuracy were close ($97.0 \pm 1.8\%$ and $93.3 \pm 4.0\%$, respectively), in an 80/20 validation split grouped by plant. The specificity was $88.2 \pm 8.3\%$, meaning that only sporadic false positives for *Xylella* were recorded; in such cases, these plants would have been referred for a confirmatory qPCR test, which is acceptable for a pre-screening tool. In the framework of managing the devastating OQDS that threatens highly susceptible Mediterranean cultivars such as Cellina di Nardò and Ogliarola Salentina, maximizing specificity is critical to prevent the unnecessary, traumatic, and economically damaging uprooting of healthy, centuries-old olive groves [42]. The model's capacity to maintain a high diagnostic sensitivity ($97.7 \pm 3.5\%$) underscores the technological robustness of the carbon-nanotube chemiresistive sensor array and is a favorable property for a screening tool, in which a false negative (an infected plant left undetected) is the more costly error. The false negatives were preferentially associated with a subset of *Xf*+ plants whose sampled tissue had a low or undetectable bacterial load. Several of the misclassified plants were highly susceptible Cellina di Nardò trees from a single Apulian orchard (field 3, Uggiano La Chiesa) which, at the reference qPCR, had returned low or undetectable bacterial DNA in leaf and/or woody tissue, indicating that the volatile signal weakens near the molecular detection limit. In these plants, the bacterial load was close to the detection limit of the molecular test, a condition under which it is unlikely that the emission of volatile compounds had already deviated from the profile of healthy plants; therefore, these false negatives largely coincided with plants having a low bacterial load. *Xf* is confined to the xylem and distributed unevenly within the canopy, and its load varies spatially and seasonally, so a particular twig sampled for qPCR may fall below the molecular detection limit even in a plant that is actually infected. The volatile signal reflects the plant's systemic physiological response to infection rather than the local bacterial load of a single twig, since xylem colonization induces water stress [43] and defense responses that alter the emission of volatile compounds throughout the entire plant [33]. However, misclassifications were not restricted to low-titre plants: some involved plants with a medium-to-high bacterial load, as evidenced by qPCR Cycle threshold (Ct) values of 30.6, 30.1, and 27.2 for the 'Cellina di Nardò' plant and 30.0, 25.3, and 23.3 for the 'Ogliarola Salentina' plant (for leaf tissue, and woody tissue processed via Quick-Pick and CTAB extraction, respectively). According to established diagnostic scales [44,45], Ct values below 35 clearly denote a medium-to-high *Xylella fastidiosa* concentration, with values in woody tissue ($Ct \leq 27$) indicating a particularly high bacterial load. This demonstrates that a low bacterial titer is not the sole source of diagnostic error and highlights the contribution of the intrinsic variability inherent to a non-specific chemiresistive array [40,41].

Furthermore, channels ch3–ch5, ch9–ch11, and ch6–ch8 contributed most to the discrimination and separate the two classes consistently, indicating that the infection is associated with a reproducible, though not yet chemically resolved, VOC-related sensor-response pattern [34,36]. A closer inspection of the importance profile suggests that the dominant

weight assigned to channel 40 should not be read as evidence of a chemically meaningful contribution. Channels ch38, ch39, and ch40 share the same functionalization and are therefore expected to carry replicate information; in the present dataset, however, channel 40 does not covary with the other two ($r = -0.203$, against $r = 1.000$ between channels 38 and 39) and shows a standard deviation more than twenty times larger than that of any other active channel. Moreover, the variability of this channel across sampling sites of the same phytosanitary status exceeds by more than thirty times the difference between the medians of the two classes, so that its response cannot be regarded as informative of the infection.

Importance estimates derived from artificial neural networks are known to depend on the method adopted and to diverge, at times substantially, from the true contribution of the input variables [46,47]. The discrepancy observed here between channels carrying identical chemical information indicates that the ranking in Figure 6 cannot be read as discriminant power alone; chemiresistive gas sensors additionally show run-to-run variability in their response [40,41]. Consistently, the permutation importance was broadly distributed across the array, with a large run-to-run variability and no single dominant channel; the most consistently informative channel (Channel 9) belonged to the ch9–ch11 triplet, which also showed one of the highest univariate discriminations. The discrimination therefore does not rely on any individual sensing element, but on the distributed and partly redundant response of the array as a whole. The possibility that the classifier discriminates the geographical origin of the samples rather than the infection was addressed by repeating the analysis within Apulia alone. The separation between *Xf*+ and *Xf*− plants increased for fourteen of the fifteen triplicates, indicating that the between-region contrast acted as a source of variability rather than as the basis of the discrimination. Two triplicates behaved differently from the others: channels ch25–ch27 separated the classes only within Apulia, and channels ch35–ch37 in neither comparison, which would be difficult to reconcile with a purely geographical signal. The residual confounding lies at the level of the individual orchard and of the acquisition session and cannot be resolved with the present sampling design: the healthy Apulian controls come from a single orchard and number only twenty plants. Crucially, the neural network successfully filtered the complex background noise of healthy plant emissions and baseline drifts despite operational challenges, such as environmental temperature and humidity fluctuations inherent to open-field and pot testing across different plant ages and phenological stages [48,49].

Some limitations should nevertheless be acknowledged. First, the phytosanitary status is partially confounded with the site, the cultivar, and the sampling session, since, within the defined area of Salento, there are no longer any olive trees assumed to be *Xf*-free belonging to susceptible cultivars, and healthy reference samples had to be collected elsewhere; similarly, neither the age of the trees nor the agronomic management could be controlled or recorded. This confounding is inherent in field studies involving a quarantine pathogen in an active phase of spread, and its effect on the present results was directly verified through the intra-Apulian analysis, in which discrimination was maintained. However, the Ogliarola Barese and Leccino cultivars were analyzed only among *Xf*− plants, while all *Xf*+ material came from a single region (Puglia); it therefore remains to be determined, through independent validation trials conducted in geographically distinct areas, whether the results of this study can be generalized to other cultivars, regions, and *Xf* subspecies. Second, although the plant-grouped design kept all replicate acquisitions of a plant within the same subset and thus prevented information leakage between the training and test subsets, the performance was estimated over repeated random 80/20 partitions rather than by a full plant-level cross-validation [50]. Plant-level cross-validation and external validation on independent olive groves are therefore necessary prior to operational use.

Furthermore, *Xf* is unevenly distributed within the canopy, and qPCR itself is prone to false negatives in the presence of a low bacterial load or PCR inhibitors [13,51].

Based on the results obtained in this study, the e-nose represents a promising proof-of-concept, point-of-care technology for the rapid screening of plant material destined for commercial exchange. Future studies should focus on the extensive validation of this tool and its performance compared with established portable diagnostic systems, such as Loop-Mediated Isothermal Amplification (LAMP). Nevertheless, the e-nose is not intended to replace molecular diagnostic methods [25]. Instead, it should be regarded as a complementary screening tool, particularly valuable in contexts where laboratory-dependent qPCR assays are not readily accessible. Furthermore, it may facilitate the selection and prioritization of samples requiring confirmatory qPCR testing, thereby improving the efficiency of surveillance and phytosanitary monitoring programs.

5. Conclusions

Since the e-nose employed in this study is a non-specific device, the chemical composition of the *Xylella fastidiosa*-associated volatilome cannot be resolved from its output. To further consolidate the chemical characterization of the *Xf* volatilome, future research will focus on employing ultra-high-resolution analytical techniques, such as Proton-Transfer-Reaction Time-of-Flight Mass Spectrometry (PTR-ToF-MS). As a result of its high sensitivity and real-time monitoring capabilities without sample fragmentation, this instrument will allow for the precise validation of the functional groups of previously identified VOCs. The aim will be to define a unique, ultra-early volatile signature associated with the pathogen infection, laying the groundwork for developing high-specificity field biosensors for rapid *Xf* diagnosis.

A portable, room-temperature carbon-nanotube electronic nose coupled with a Shallow Neural Network discriminated *Xf*-infected from healthy olive trees directly in commercial orchards, across four cultivars, four Italian regions, and uncontrolled environmental conditions, with 93.3 $\pm$ 4.0% test accuracy (mean $\pm$ SD). The discriminant information is carried by the array as a whole rather than by individual sensing channels, and it persists when the between-region contrast is removed. On this basis, the device qualifies as a proof-of-concept, portable, and reagent-free pre-screening tool for *Xf* surveillance.

Author Contributions: Conceptualization, F.A., C.C., F.P. and R.M.; methodology, F.A., C.C., F.P. and R.M.; software, C.C., L.M. and S.F.; validation, C.C., L.M. and F.P.; formal analysis, R.M., A.M. and S.V. (Simone Vasta); investigation, F.A., C.C., F.P., R.M. and G.T.; resources, F.A., N.P. and S.L.; data curation, R.M., C.C. and S.F.; writing—original draft preparation, R.M., F.A., L.M. and S.V. (Simona Violino); writing—review and editing, R.M., F.A., S.L., N.P. and S.V. (Simona Violino); visualization, F.A., C.C., F.P. and R.M.; supervision, F.A., C.C. and F.P.; project administration, F.A., S.L. and N.P.; funding acquisition, F.A., S.L. and N.P. All authors have read and agreed to the published version of the manuscript.

Funding: This research was supported by the Italian Ministry of Agriculture, Food Sovereignty and Forests (MASAF) project DIACOX (D.M. n. 664531/2022).

Data Availability Statement: The original contributions presented in this study are included in the article. Further inquiries can be directed to the corresponding author.

Acknowledgments: The authors gratefully acknowledge: Pio Federico Roversi (CREA-DC) for laboratory and diagnostic support; Enzo Perri, Samanta Zelasco, Veronica Vizzarri, Cinzia Benincasa, and Giuseppe Cruceli (CREA-OFA) for germplasm and field assistance; and Franco Nigro (UniBa), Pasquale Venerito (CRSFA Locorotondo), Marcello Simone (IS Pantanelli Ostuni), Pietro Loparco, Michele Trotti, Francesco Panizzi (UniSalento), and Cosimo Taiti (SEMIA/UniFI) for field access and sampling support. The authors have reviewed and edited the output and take full responsibility

for the content of this publication. This work was carried out within the Ph.D. programme in "Engineering for Energy and Environment" (XXXVII cycle) of Rossella Manganiello at the University of Tuscia, Viterbo, Italy.

Conflicts of Interest: The authors declare no conflicts of interest.

References

1. Saponari, M.; Boscia, D.; Altamura, G.; Loconsole, G.; Zicca, S.; D'Attoma, G.; Morelli, M.; Palmisano, F.; Saponari, A.; Tavano, D.; et al. Isolation and Pathogenicity of *Xylella fastidiosa* Associated to the Olive Quick Decline Syndrome in Southern Italy. *Sci. Rep.* **2017**, *7*, 17723. [CrossRef] [PubMed]
2. Saponari, M.; D'Attoma, G.; Abou Kubaa, R.; Loconsole, G.; Altamura, G.; Zicca, S.; Rizzo, D.; Boscia, D. A New Variant of *Xylella fastidiosa* Subspecies *multiplex* Detected in Different Host Plants in the Recently Emerged Outbreak in the Region of Tuscany, Italy. *Eur. J. Plant Pathol.* **2019**, *154*, 1195–1200. [CrossRef]
3. Cornara, D.; Boscia, D.; D'Attoma, G.; Digiaro, M.; Ligorio, A.M.; Loconsole, G.; Minutillo, S.A.; Montilon, V.; Palmisano, F.; Ragone, G.; et al. An Integrated Strategy for Pathogen Surveillance Unveiled *Xylella fastidiosa* ST1 Outbreak in Hidden Agricultural Compartments in the Apulia Region (Southern Italy). *Eur. J. Plant Pathol.* **2025**, *171*, 277–285. [CrossRef]
4. Schneider, K.; Van der Werf, W.; Cendoya, M.; Mourits, M.; Navas-Cortés, J.A.; Vicent, A.; Oude Lansink, A. Impact of *Xylella fastidiosa* subspecies pauca in European olives. *Proc. Natl. Acad. Sci. USA* **2020**, *117*, 9250–9259. [CrossRef] [PubMed]
5. Cornara, D.; Bosco, D.; Fereres, A. *Philaenus spumarius*: When an Old Acquaintance Becomes a New Threat to European Agriculture. *J. Pest Sci.* **2018**, *91*, 957–972. [CrossRef]
6. Calderoni, F.; Petrontino, A.; Frem, M.; Fucilli, V.; Bozzo, F. Economic and Social Impacts of Olive Quick Decline Syndrome: Analysing Data from the Italian Farm Accountancy Network. *Plant Pathol.* **2025**, *74*, 1010–1023. [CrossRef]
7. Aprile, A.; Negro, C.; Sabella, E.; Luvisi, A.; Nicolì, F.; Nutricati, E.; Vergine, M.; Miceli, A.; Blando, F.; De Bellis, L. Antioxidant Activity and Anthocyanin Contents in Olives (cv Cellina di Nardò) during Ripening and after Fermentation. *Antioxidants* **2019**, *8*, 138. [CrossRef] [PubMed]
8. La Notte, P.; Saponari, M.; Mousavi, S.; Mariotti, R.; Abou Kubaa, R.; Nikbakht, R.; Melcarne, G.; Specchia, F.; Altamura, G.; Ligorio, A.; et al. A Survey in Natural Olive Resources Exposed to High Inoculum Pressure Indicates the Presence of Traits of Resistance to *Xylella fastidiosa* in Leccino Offspring. *Front. Plant Sci.* **2024**, *15*, 1457831. [CrossRef] [PubMed]
9. D'Addabbo, A.; Matarrese, R.; Lovergine, F.; Refice, A.; Belmonte, A.; Bovenga, F.; Gallo, A.; Amoia, S.S.; Kubaa, R.A.; Mita, G.; et al. Toward an Operational System for Automatically Detecting *Xylella fastidiosa* in Olive Groves Based on Hyperspectral and Thermal Remote Sensing Data. *Remote Sens.* **2025**, *17*, 1372. [CrossRef]
10. Cagnarini, C.; De Angelis, P.; Liberati, D.; Valentini, R.; Falanga, V.; Valentini, F.; Dongiovanni, C.; Carrieri, M.; Chiriacò, M.V. Physiological Response of Olive Trees Under *Xylella fastidiosa* Infection and Thymol Therapy Monitored Through Advanced IoT Sensors. *Plants* **2025**, *14*, 1380. [CrossRef] [PubMed]
11. Castrignanò, A.; Belmonte, A.; Antelmi, I.; Quarto, R.; Quarto, F.; Shaddad, S.; Sion, V.; Muolo, M.R.; Ranieri, N.A.; Gadaleta, G.; et al. Semi-Automatic Method for Early Detection of *Xylella fastidiosa* in Olive Trees Using UAV Multispectral Imagery and Geostatistical-Discriminant Analysis. *Remote Sens.* **2021**, *13*, 14. [CrossRef]
12. Di Nisio, A.; Adamo, F.; Acciani, G.; Attivissimo, F. Fast Detection of Olive Trees Affected by *Xylella fastidiosa* from UAVs Using Multispectral Imaging. *Sensors* **2020**, *20*, 4915. [CrossRef] [PubMed]
13. Román-Écija, M.; Olivares-García, C.; Landa, B.B.; Navas-Cortés, J.A. Extent of Stem Colonization of Spanish *Xylella fastidiosa* Strains in Olive: A Proximal Sensing Approach for Early Detection of Infection. *Plant Dis.* **2026**, *110*, 741–753. [CrossRef] [PubMed]
14. MacDougall, S.; Bayansal, F.; Ahmadi, A. Emerging Methods of Monitoring Volatile Organic Compounds for Detection of Plant Pests and Disease. *Biosensors* **2022**, *12*, 239. [CrossRef] [PubMed]
15. Fundurulic, A.; Faria, J.M.S.; Inácio, M.L. Advances in Electronic Nose Sensors for Plant Disease and Pest Detection. *Eng. Proc.* **2023**, *48*, 14. [CrossRef]
16. Kriz, P.; Sikora, P.; Riha, K.; Burget, R. Unveiling the Smell Inspector and Machine Learning Methods for Smell Recognition. In *Proceedings of the 2023 15th International Congress on Ultra Modern Telecommunications and Control Systems and Workshops (ICUMT), Ghent, Belgium, 30 October–1 November 2023*; IEEE: Piscataway, NJ, USA, 2023; pp. 182–187.
17. Benos, L.; Tagarakis, A.C.; Dolias, G.; Berruto, R.; Kateris, D.; Bochtis, D. Machine Learning in Agriculture: A Comprehensive Updated Review. *Sensors* **2021**, *21*, 3758. [CrossRef] [PubMed]
18. Ye, Z.; Liu, Y.; Li, Q. Recent Progress in Smart Electronic Nose Technologies Enabled with Machine Learning Methods. *Sensors* **2021**, *21*, 7620. [CrossRef] [PubMed]
19. Peters, R.; Beijer, N.; 't Hul, B.; Bruijns, B.; Munniks, S.; Knotter, J. Evaluation of a Commercial Electronic Nose Based on Carbon Nanotube Chemiresistors. *Sensors* **2023**, *23*, 5302. [CrossRef] [PubMed]

20. Tiberini, A.; Costa, C.; Pallottino, F.; Figorilli, S.; Donati, L.; Manglli, A.; Tocci, F.; Vasta, S.; Manganiello, R.; Antonucci, F. Preliminary Early Detection of Tomato Spotted Wilt Virus Using IoT Digital Electronic Nose in Combination with Artificial Intelligence Algorithms. In Proceedings of the XX International Plant Protection Congress (IPPC)—Healthy Plants Support Human Welfare, Athens, Greece, 1–5 July 2024; p. 277.
21. Infantino, A.; Spampinato, F.; Costa, C.; Manganiello, R.; Tocci, F.; Valente, M.T.; Bechini, S.; Groli, E.; Ravaglia, S.; Vaccino, P. Use of a Portable E-Nose for the Analysis of Bread Wheat Kernel Samples Artificially Infected with *Fusarium graminearum* and *Fusarium culmorum*. *J. Plant Pathol.* **2025**, *107*, 1631–1632. [CrossRef]
22. IPPC Secretariat. *Diagnostic Protocols for Regulated Pests, DP 25: Xylella fastidiosa (ISPM 27)*; 2025; Revised 10 March 2025; International Plant Protection Convention (IPPC) Secretariat; FAO: Rome, Italy; Available online: https://www.ippc.int/en/publications/86498/ (accessed on 30 July 2026).
23. Karakaya, D.; Ulucan, O.; Turkan, M. Electronic Nose and Its Applications: A Survey. *Int. J. Autom. Comput.* **2020**, *17*, 179–209. [CrossRef]
24. Schroeder, V.; Savagatrup, S.; He, M.; Lin, S.; Swager, T.M. Carbon Nanotube Chemical Sensors. *Chem. Rev.* **2019**, *119*, 599–663. [CrossRef] [PubMed]
25. EPPO. PM 7/24 (5) *Xylella fastidiosa*. *EPPO Bull.* **2023**, *53*, 205–276. [CrossRef]
26. Martín-Vertedor, D.; Tian, C.; Lozano, J.; Monago-Maraña, O.; Chiappini, F.; Pérez-Nevado, F. Discrimination of Spanish-Style Green Olives Inoculated with Undesirable Microbiota Using E-Nose, Chemometrics and Volatile Compound Profiles. *Foods* **2026**, *15*, 934. [CrossRef] [PubMed]
27. Alrashdi, I.; Abozeid, A. An efficient deep-learning model for olive tree diseases diagnosis in Al-Jouf region. *Alex. Eng. J.* **2025**, *130*, 709–723. [CrossRef]
28. Agarap, A.F. Deep Learning Using Rectified Linear Units (ReLU). *arXiv* **2018**, arXiv:1803.08375.
29. Tharwat, A. Classification Assessment Methods. *Appl. Comput. Inform.* **2021**, *17*, 168–192. [CrossRef]
30. Chollet, F. Keras: Deep Learning Library for Python. 2015. Available online: https://github.com/fchollet/keras (accessed on 1 June 2026).
31. Abadi, M.; Agarwal, A.; Barham, P.; Brevdo, E.; Chen, Z.; Citro, C.; Corrado, G.S.; Davis, A.; Dean, J.; Devin, M.; et al. TensorFlow: Large-Scale Machine Learning on Heterogeneous Distributed Systems. *arXiv* **2016**, arXiv:1603.04467.
32. Pedregosa, F.; Varoquaux, G.; Gramfort, A.; Michel, V.; Thirion, B.; Grisel, O.; Blondel, M.; Prettenhofer, P.; Weiss, R.; Dubourg, V.; et al. Scikit-Learn: Machine Learning in Python. *J. Mach. Learn. Res.* **2011**, *12*, 2825–2830.
33. Mentana, A.; Camele, I.; Mang, S.M.; De Benedetto, G.E.; Frisullo, S.; Centonze, D. Volatolomics Approach by HS-SPME-GC-MS and Multivariate Analysis to Discriminate Olive Tree Varieties Infected by *Xylella fastidiosa*. *Phytochem. Anal.* **2019**, *30*, 623–634. [CrossRef] [PubMed]
34. Girelli, C.R.; Hussain, M.; Verweire, D.; Oehl, M.C.; Massana-Codina, J.; Avendaño-Herrera, R.; Migoni, D.; Scortichini, M.; Fanizzi, F.P. Agro-Active Endo-Therapy Treated *Xylella fastidiosa* subsp. *pauca*-Infected Olive Trees Assessed by the First 1H-NMR-Based Metabolomic Study. *Sci. Rep.* **2022**, *12*, 5973. [CrossRef] [PubMed]
35. Girelli, C.R.; Del Coco, L.; Angilè, F.; Scortichini, M.; Fanizzi, F.P. Olive Cultivars Susceptible or Tolerant to *Xylella fastidiosa* Subsp. *pauca* Exhibit Mid-Term Different Metabolomes upon Natural Infection or a Curative Treatment. *Plants* **2021**, *10*, 772. [CrossRef] [PubMed]
36. Ahmed, E.; Musio, B.; Todisco, S.; Mastrorilli, P.; Gallo, V.; Saponari, M.; Nigro, F.; Gualano, S.; Santoro, F. Non-Targeted Spectranomics for the Early Detection of *Xylella fastidiosa* Infection in Asymptomatic Olive Trees, cv. Cellina di Nardò. *Molecules* **2023**, *28*, 7512. [CrossRef] [PubMed]
37. Hazarika, S.; Choudhury, R.; Montazer, B.; Medhi, S.; Goswami, M.P.; Sarma, U. Detection of Citrus Tristeza Virus in Mandarin Orange Using a Custom-Developed Electronic Nose System. *IEEE Trans. Instrum. Meas.* **2020**, *69*, 9010–9018. [CrossRef]
38. Xu, Q.; Bai, J.; Ma, L.; Li, Z.; Tan, B.; Sun, L.; Cai, J. Identification of Multiple Symptoms of Huanglongbing by Electronic Nose Based on the Variability of Volatile Organic Compounds. *Ann. Appl. Biol.* **2023**, *183*, 181–195. [CrossRef]
39. Wang, Z.; Niu, Y.; Vashisth, T.; Li, J.; Madden, R.; Livingston, T.S.; Wang, Y. Nontargeted Metabolomics-Based Multiple Machine Learning Modeling Boosts Early Accurate Detection for Citrus Huanglongbing. *Hortic. Res.* **2022**, *9*, uhac145. [CrossRef] [PubMed]
40. Sun, F.; Sun, R.; Yan, J. Cross-Domain Active Learning for Electronic Nose Drift Compensation. *Micromachines* **2022**, *13*, 1260. [CrossRef] [PubMed]
41. Cai, M.; Xu, S.; Zhou, X.; Lu, H. Electronic Nose Humidity Compensation System Based on Rapid Detection. *Sensors* **2024**, *24*, 5881. [CrossRef] [PubMed]
42. Ciervo, M.; Scortichini, M. A Decade of Monitoring Surveys for *Xylella fastidiosa* subsp. *pauca* in Olive Groves in Apulia (Italy) Reveals a Low Incidence of the Bacterium in the Demarcated Areas. *J. Phytopathol.* **2024**, *172*, e13272. [CrossRef]

43. Surano, A.; Abou Kubaa, R.; Nigro, F.; Altamura, G.; Losciale, P.; Saponari, M.; Saldarelli, P. Susceptible and Resistant Olive Cultivars Show Differential Physiological Response to *Xylella fastidiosa* Infections. *Front. Plant Sci.* **2022**, *13*, 968934. [CrossRef] [PubMed]
44. Dupas, E.; Briand, M.; Jacques, M.-A.; Cesbron, S. Novel Tetraplex Quantitative PCR Assays for Simultaneous Detection and Identification of Xylella fastidiosa Subspecies in Plant Tissues. *Front. Plant Sci.* **2019**, *10*, 1732. [CrossRef] [PubMed]
45. Bonants, P.; Griekspoor, Y.; Houwers, I.; Krijger, M.; van der Zouwen, P.; van der Lee, T.; van der Wolf, J. Development and evaluation of a triplex TaqMan assay and next-generation sequence analysis for improved detection of *Xylella* in plant material. *Plant Dis.* **2019**, *103*, 645–655. [CrossRef] [PubMed]
46. Hooker, G.; Mentch, L.; Zhou, S. Unrestricted Permutation Forces Extrapolation: Variable Importance Requires at Least One More Model, or There Is No Free Variable Importance. *Stat. Comput.* **2021**, *31*, 82. [CrossRef]
47. Williamson, B.D.; Gilbert, P.B.; Carone, M.; Simon, N. Nonparametric Variable Importance Assessment Using Machine Learning Techniques. *Biometrics* **2021**, *77*, 9–22. [CrossRef] [PubMed]
48. Robbiani, S.; Lotesoriere, B.J.; Dellacà, R.L.; Capelli, L. Physical Confounding Factors Affecting Gas Sensors Response: A Review on Effects and Compensation Strategies for Electronic Nose Applications. *Chemosensors* **2023**, *11*, 514. [CrossRef]
49. Herrmann, P.S.D.P.; Santos Luccas, M.D.; Ferreira, E.J.; Torre Neto, A. Application of electronic nose and machine learning used to detect soybean gases under water stress and variability throughout the daytime. *Front. Plant Sci.* **2024**, *15*, 1323296. [CrossRef] [PubMed]
50. Kapoor, S.; Narayanan, A. Leakage and the Reproducibility Crisis in Machine-Learning-Based Science. *Patterns* **2023**, *4*, 100804. [CrossRef] [PubMed]
51. Dupas, E.; Legendre, B.; Olivier, V.; Poliakoff, F.; Manceau, C.; Cunty, A. Comparison of Real-Time PCR and Droplet Digital PCR for the Detection of *Xylella fastidiosa* in Plants. *J. Microbiol. Methods* **2019**, *162*, 86–95. [CrossRef] [PubMed]